New Methodological Approach for the Vanadium K-Edge X-ray Absorption Near-Edge Structure Interpretation: Application to the Speciation of Vanadium in Oxide Phases from Steel Slag

Perrine Chaurand,*,† Jérôme Rose,† Valérie Briois,‡ Murielle Salome,§ Olivier Proux,|| Vivian Nassif,+ Luca Olivi,# Jean Susini,§ Jean-Louis Hazemann,⊥ and Jean-Yves Bottero†

CEREGE UMR CNRS/Université Paul Cézanne Aix-Marseille III, Europôle de l'Arbois, BP80, 13545 Aix en Provence Cedex 4, France, SOLEIL, L'Orme des merisiers, BP48, Saint Aubin, 91192 Gif sur Yvette, France, European Synchrotron Radiation Facility, BP220, F-38043 Grenoble, Cedex 9, France, CEA/Grenoble, DRFMC/SP2M/NRS, 17 avenue des Martyrs, F-38054 Grenoble Cedex 9, France, Laboratoire de Géophysique Interne et Tectonophysique, UMR CNRS/Université Joseph Fourier, 1381 rue de la Piscine, Domaine Universitaire, F-38400 Saint-Martin-D'Hères, France, Sincrotrone Trieste S.C.p.A., Strada Statale 14, Km 163.5, 34012 Basovizza, Trieste, Italy, and Laboratoire de Cristallographie, CNRS, 25 avenue des Martyrs, BP166, F-38042 Grenoble Cedex 9, France

Received: May 24, 2006; In Final Form: December 1, 2006

This paper presents a comparison between several methods dedicated to the interpretation of V K-edge X-ray absorption near-edge structure (XANES) features. V K-edge XANES spectra of several V-bearing standard compounds were measured in an effort to evaluate advantages and limits of each method. The standard compounds include natural minerals and synthetic compounds containing vanadium at various oxidation state (from +3 to +5) and in different symmetry (octahedral, tetrahedral, and square pyramidal). Correlations between normalized pre-edge peak area and its centroid position have been identified as the most reliable method for determining quantitative and accurate redox and symmetry information for vanadium. This methodology has been previously developed for the Fe K edge. It is also well adapted for the V K edge and is less influenced by the standard choice than other methods. This methodology was applied on an "environmental sample," i.e., a well-crystallized leached steel slag containing vanadium as traces. Micro-XANES measurements allowed elucidating the microdistribution of vanadium speciation in leached steel slag. The vanadium exhibits an important evolution from the unaltered to the altered phases. Its oxidation state increases from +3 to +5 together with the decrease of its symmetry (from octahedral to tetrahedral).

Introduction

Vanadium is a metal that exhibits a wide range of oxidation states (from 0 to +5): the most common are +3, +4, and +5.[1,2] Trivalent V has the electron configuration $3s^2 3p^6 3d^2$ and occurs commonly in octahedral symmetry (O_h). Tetravalent V has the electron configuration $3s^2 3p^6 3d^1$, and its common symmetry is square pyramidal (P_y) and octahedral (O_h). And, pentavalent V has the electron configuration $3s^2 3p^6 3d^0$ and presents different kinds of symmetry: tetrahedral (T_d), square pyramidal (P_y) and octahedral (O_h).[3] The multiple oxidation states and symmetries of vanadium confer it a high complexity. Evans[4] surveyed the crystal chemistry of vanadium minerals and examined the types of V coordination polyhedra that they contain. More recently, Schindler et al.[5] discussed bond-length variation in ($V^{i+}O_n$) polyhedra ($i = 3, 4, 5$; $n = 5, 6$). Finally, Zavalij et al.[6] and Guili et al.[7] studied the crystal chemistry of vanadium oxides and vanadium in silicate glasses, respectively.

Vanadium systems as amorphous V_2O_5, $V_2O_5-P_2O_5$ glasses, $Li_xV_2O_5$ or $LiNiVO_4$ systems, vanadium mesoporous silica, or vanadium supported on titanium have been extensively studied since they are good candidates for making reversible cathodes in lithium batteries or are commonly used as catalyst for a number of industrially important reactions. Moreover borosilicate glasses containing vanadium are interesting in the frame of vitrification of sulfur-bearing radioactive wastes for long-term storage because adding V_2O_5 to borosilicate formulations seems to improve sulfur solubility in the melt (see references in Table 1). A better knowledge of vanadium speciation (oxidation state and symmetry) in these materials is one of the key points for a better understanding of their physical and chemical properties. X-ray absorption near-edge structure (XANES) spectroscopy is a well-adapted method to identify vanadium speciation. XANES is the region of the X-ray absorption spectrum (XAS) within ~50 eV of threshold and includes the pre-edge, the edge, and the first oscillations. This region has long been known to be rich in chemical and structural information of the absorber atom.[8,9] An extensive review dealing with the shape and energy position of V K-edge XANES features for several compounds[10] has been published. However, the accurate physical and chemical interpretation of all features is still difficult.

A review of the XANES interpretation methods permitting oxidation state and/or symmetry determination is presented in

* To whom correspondence should be addressed. E-mail: chaurand@cerege.fr. Phone: +0033 (0)4 42 97 15 43. Fax: +0033 (0)4 42 97 15 59.
† CEREGE.
‡ SOLEIL.
§ European Synchrotron Radiation Facility.
|| CEA/Grenoble.
+ Laboratoire de Géophysique Interne et de Tectonophysique.
# Sincrotrone Trieste S.C.p.A.
⊥ Laboratoire de Cristallographie.

10.1021/jp063186i CCC: $37.00
Published on Web 04/13/2007

TABLE 1: Interpretation Methods of XANES Features

interpretation method	oxidation state	symmetry	element	material and references
absorption edge position	x		V	$LiNiVO_4$,[42] borosilicate waste glasses,[41] vanadium oxides,[10] $V+TiO_2$ hybrid samples,[48] V_2O_5 aerogel cathodes,[40] V tetracyanoethylene,[43] $LiNiVO_4$,[39] blood cells of ascidians,[49] V_2TiO_5,[50] V-containing bromoperoxidase,[51] vanadates,[52] (Ti, V)O_2 rutile solid solutions[36]
pre-edge peak intensity		x	V	borosilicate waste glasses,[41] vanadium-oxygen compounds,[53] $Li_xV_2O_5$ xerogels,[19] mesoporous silica MCM-41,[54] $V+TiO_2$ hybrid samples,[48] V_2O_5 aerogel cathodes,[40] V tetracyanoethylene,[43] $LiNiVO_4$,[39] V-mesoporous molecular sieves,[55] V_2TiO_5,[50] V-containing bromoperoxidase,[51] vanadates,[52] CoV_2O_6/Li battery[56]
	x	x	V	natural basaltic glasses[14]
	x	x	Cr^{3+}/Cr^{6+}	environmental samples,[44] Portland cement[57]
normalized pre-edge peak height vs absolute position	x	x	V	silicate glasses[7]
		x	Ti^{4+}	silicate glasses and melts,[17] crystalline and glassy fresnoites ($Ba_2TiOSi_2O_7$)[16]
normalized pre-edge peak area vs centroid position	x	x	Fe^{2+}/Fe^{3+}	minerals with variable Fe^{2+}/Fe^{3+} ratio,[20] natural Fe minerals,[22] ferrosilicate glasses[18,58]
	x	x	Mn	oxides and silicates, natural or synthetic containing Mn[35]

Table 1. In most of the studies, the vanadium oxidation state is determined through the position of the absorption edge, which shifts to higher energies with an increasing valence state. The energy shifts, so-called chemical shifts, are found to follow Kunzl's law in Wong et al.[10] and to vary linearly with the valence of the absorbing vanadium atom. However, this "simple" empirical law is not generally well adapted because many factors influence the spectral shape (multiscattering effects, multielectronic effects, matrix effects, etc.).[11]

The intensity of the pre-edge peak is generally used qualitatively to obtain information on symmetry site. The pre-edge feature is related to electronic transitions from 1s core levels to the empty 3d levels, more or less 4p hybridized by the V ligands (probing thus the density of the lowest unoccupied states). These electronic transitions become allowed when the inversion center is lost. In this case, the loss of symmetry permits partial overlapping and mixing of the unfilled d states of the metal with the 4p orbital of the metal. Pre-edge peak intensity will be virtually zero in the case of regular octahedral symmetry (O_h) around the absorber, whereas it will have a higher intensity in the case of tetrahedral symmetry (T_d). Actually, as the main transitions at the K-edge are electric dipolar allowed, it is assumed that the pre-edge peak area could be correlated to the percentage of metal 4p atomic orbital hybridized with the metal 3d atomic orbitals[12] (even if this statement has been recently questioned[13]).

The pre-edge peak intensity helps to determine the vanadium valence only in particular conditions,[14] contrary to chromium for which the pre-edge peak is very weak for octahedral Cr^{3+} and very intense for tetravalent Cr^{6+}.[15] Giuli et al.[7] proposed an original approach and consider the pre-edge intensity as well as its absolute position to determine both the vanadium oxidation state and its symmetry. This methodology was initially developed by Farges et al.[16−18] to provide information on the local structure around Ti^{4+} in crystalline and glassy fresnoites and in silicate glasses and melts. The only pre-edge peak position is generally insufficient to evaluate accurately vanadium oxidation state, except for some studies.[10,19] A very interesting methodology was followed by Wilke et al.[20,21] and Petit et al.[22] to estimate the Fe^{3+}/Fe^{2+} ratio in minerals. They consider that the most useful characteristics for determining Fe oxidation state and symmetry are the position of the pre-edge peak centroid and its integrated area. To our knowledge this reliable interpretation method was never applied for V K-edge XANES spectra.

The determination of vanadium oxidation state and symmetry from XANES features could be based on several methods (Table 1). The difficulty lies in the choice of the most suitable approach. The present paper presents a comparative evaluation of all the interpretation methods used. Their own pertinence, accurateness, reliability, and limits will be discussed. The final objective is to identify and suggest a precise and rigorous methodology devoted to the quantitative evaluation of vanadium speciation (oxidation state and symmetry) from XANES features. The selected interpretation method is based on correlations between the normalized total area and the centroid of the energy position of pre-edge features. Results of a high-resolution XANES spectroscopy study of vanadium in several standard compounds that possess a wide range of oxidation state and symmetry are presented.

The selected method is well adapted for unknown complex matrix containing vanadium at very low content, as in some natural systems or industrial residues, i.e., typical samples studied in Environmental Sciences. As an example, the speciation of vanadium within altered basic oxygen furnace (BOF) steel slag was determined. BOF steel slag is a residue from the basic converter in steel-making operations and is partially reused as an aggregate in road constructions.[23] It consists of a well-crystallized and heterogeneous matrix composed of dicalcium-silicate (Ca_2SiO_4), dicalciumferrite ($Ca_2Fe_2O_5$), a solid solution (Fe, Mn, Mg, Ca)O, and calcite ($CaCO_3$).[24,25] This industrial residue is an interesting matrix to test the selected interpretation method because it contains vanadium at trace amounts, from 430 to 1700 mg/kg.[26] Moreover the crystallized phases are sensitive to water contact, and the composition of the solid matrix is susceptible to change during alteration. The vanadium release is relatively high during laboratory-scale leaching tests, and an evolution of its speciation within the solid phase

TABLE 2: Local Structure Information of the V Crystallographic Sites for Standard Compounds

compounds	formal valence	bond type	no. bonds	symmetry[a]	bond distance (Å)	references
V metal	0	V−V	8		2.622	Wong et al., 1984[10]
coulsonite						
FeV_2O_4	3	V−O	6	O_h	1.9782	Chicagov, 1990[59]
V_2O_4	4	V−O	6	O_h	1.76, 1.86, 1.87, 2.01, 2.03, 2.05	Wong et al., 1984[10]
cavansite						
$Ca(VO)(Si_4O_{10})\cdot 4H_2O$	4	V−O	5	P_y	1.6, 1.98 × 4	Evans et al., 1973[60]
pascoite $Ca_3(V_{10}O_{28})\cdot 17H_2O$	5	V−O	6	O_h	1.598−2.312	Hughes et al., 2005[61]
V_2O_5	5	V−O	5	P_y	1.585, 1.780, 1.878, 1.878, 2.021	Wong et al., 1984[10]
Na_3VO_4	5	V−O	4	T_d	1.677, 1.696 × 3	Hardcastle et al., 1991[62]
vanadinite $Pb_5(VO_4)_3Cl$	5	V−O	4	T_d	1.7	Dai et al., 1989[63]

[a] O_h, octahedral; T_d, tetrahedral; P_y, square pyramidal.

(oxidation state and/or symmetry) is suspected.[27] Indeed the solubility of this element as well as its toxicity evolves with its redox chemistry: going from reducing to oxic environment leads to an increase in its solubility[28] with vanadate (V^{5+}) as the prevailing form.

Experimental Section

Standard Compounds. The methodology developed in this paper is based on comparisons with several standard compounds of well-known crystal structure. Vanadium in these compounds exhibits a wide range of formal oxidation state, from V^{3+} to V^{5+}, and symmetry (octahedral, tetrahedral, and square pyramidal). The studied compounds studied include the oxides V_2O_4 and V_2O_5, the compound Na_3VO_4, and vanadium-bearing minerals such as coulsonite FeV_2O_4, pascoite $Ca_3(V_{10}O_{28})\cdot 17H_2O$ and metarossite $CaV_2O_6\cdot 4H_2O$, cavansite $Ca(VO)(Si_4O_{10})\cdot 4H_2O$, and vanadinite $Pb_5(VO_4)_3Cl$ (see structural information in Table 2). All standard compounds were checked for purity by X-ray diffraction and X-ray fluorescence.

Leached Steel Slag. The studied steel slag contains 690 mg/kg of vanadium. A grain of several centimeters was leached for 26 days using a modified Soxhlet extractor named CTG-Leachcrete.[29] The principle of this dynamic leaching device is to produce water vapor in a boiler balloon flask connected to a leaching cell (filled with deionized water), regulated in temperature (25 °C). After 26 days of leaching, the altered layer reached 200 μm thick. A sample of steel slag was also subjected to natural aging in a lysimeter of 1 m^3 placed outdoors for a period of 2 years (sample provided by the Laboratoire Central des Ponts et Chaussées, France). Leached grains were sawed with a diamond wire saw before micro-XANES measurements to display the altered region (surface layer) and the unaltered region (sound core).

XANES Spectra Measurement. V K-edge XANES spectra of standard compounds were collected on beamline BL-11.1 of the Elettra storage ring (Triestre, Italy) operated at 2 GeV with a current of 150 mA and on beamline CRG-FAME[30,31] at the ESRF facility (Grenoble, France), a storage ring operated at 6 GeV with a current ranging from 150 to 200 mA. Spectra were collected in the transmission mode or in the fluorescence mode (according to the vanadium content in the samples).

The appropriate amount of powdered standard compounds were mixed with boron nitride (BN) to reach a dilution level corresponding to optimal sample thickness for transmission experiments (edge jump close to 1), and each mixture was compressed into a pellet (of 16 or 5 mm diameter) in ambient air. In the fluorescence mode, XANES spectra of diluted samples were collected with the sample positioned 45° with respect to the beam. The fluorescence yield was measured with a multielement solid-state detector that collected X-rays only in an electronically gated energy interval appropriate for fluorescence X-rays of the absorbing element (7 elements on BL-11.1 and 30 elements on CRG-FAME).

Micro-XANES spectra were collected in the fluorescence mode on beamline ID21[32] at the ESRF facility (Grenoble, France). The ID21 beamline is dedicated to X-ray spectroscopy and imaging at the sub-micrometer level. X-ray fluorescence emitted from the sample was analyzed using a high-energy resolution germanium solid-state detector. The beam energy was set to 5500 eV to ensure good fluorescence yield for vanadium and a spatial resolution of 0.35 × 1 μm was achieved. V-rich regions of interests (ROI) were selected in the altered region (surface layer) and in the unaltered region (sound core) of leached grains to perform XANES spectra.

Typical XANES spectrum was acquired from 5445 to 5550 eV with 0.2 eV monochromator steps on beamline ID21 and from 5300 to 5600 eV with 0.1 eV monochromator step over the pre-edge and edge region on beamlines BL-11.1 and CRG-FAME. The recording of V K-edge XANES spectra was successful despite the very low vanadium content in steel slag (690 mg/kg) and the high contents of titanium (the Ti Kβ and V Kα fluorescence lines are superimposed) and calcium (the large Ca fluorescence counts saturate the fluorescence detector).

XANES Data Analysis. *Normalization.* To compare quantitatively the intensity of absorption features in various compounds, the experimental V K-edge spectra were normalized using standard edge step normalization procedure.[10] All the XANES spectra were reduced by background subtraction with a linear function (for standard compounds) or a modified Victoreen function (for steel slag, because of the presence of Ti) and normalized using the point of inflection of the first EXAFS oscillations as a unit. The absolute zero of energy is taken with respect to the first point of inflection of the vanadium metal derivative spectrum (called E_0), which corresponds by convention to the excitation of an inner shell electron to an empty state just above the Fermi edge of the V metal.[33] For each spectrum, the vanadium foil was scanned to correct for energy shift and to obtain energy calibrated spectra in a consistent fashion.

Absorption Edge Position. For convenience the location of the absorption edge is usually defined as the energy of the first point of inflection of the principal absorption edge (given by the maximum in the derivative spectrum) or as the energy measured half way up the edge step. In the present study, we measured the edge energy half way up the normalized-edge step, i.e., where the absorption is equal to 0.5 ($E_{1/2}$) (Table 3, column 9).

Pre-Edge Analysis. Pre-edge peak analysis was carried out following a procedure inspired from the procedure reported by

TABLE 3: Pre-Edge Characteristics for V Standard Compounds (XANES)

		pre-edge peak[a]						main edge
compounds	monochromator crystals	normalized intensity	absolute position (eV)	component position (eV)	area	total area	centroid (eV)	$E_{1/2}$ (eV)
coulsonite	Si-(111)	0.06	3.7	2.3	0.04	0.21	3.7	12.9
				4.0	0.17			
	Si-(220)	0.07	3.9	2.6	0.06	0.21	3.7	12.8
				4.1	0.15			
V_2O_4	Si-(220)	0.31	4.4	4.1	0.20	1.44	5.1	13.12
				5.3	1.24			
cavansite	Si-(220)	0.66	3.9	3.9	1.12	1.46	4.1	13.6
				4.8	0.34			
pascoite	Si-(111)	0.48	5.3	3.3	0.14	1.23	5.3	15.4
				5.2	0.86			
				6.9	0.23			
	Si-(220)	0.56	5.1	3.2	0.14	1.34	5.2	15.1
				5.1	0.97			
				7.0	0.23			
V_2O_5	Si-(111)	0.59	5.4	3.0	0.10	1.94	5.9	15.6
				5.4	0.94			
				6.8	0.90			
	Si-(220)	0.78	5.3	2.8	0.07	2.15	5.8	15.3
				5.3	1.25			
				6.7	0.83			
Na_3VO_4	Si-(220)	1.15	4.8	3.2	0.46	2.71	4.8	15.0
				4.8	1.85			
				6.8	0.40			
vanadinite	Si-(111)	0.92	4.6	4.5	1.82	2.41	5.0	16.1
				6.0	0.39			
				8.0	0.20			
	Si-(220)	1.16	4.4	4.4	2.12	2.55	4.8	16.3
				6.0	0.24			
				8.1	0.19			

[a] Normalized and fitted according to the procedure described previously. The errors of the energy position are of the order of ±0.05 eV.

Wilke et al.,[20] Petit et al.,[22] and Galoisy et al.[34] for Fe K-edge data and by Farges for Mn K-edge data.[35]

To extract the pre-edge feature, the contribution of the edge jump to the pre-edge was modeled using a function that was used to interpolate the background using the data several electronvolts before and after the pre-edge feature (baseline)[20] (Figure 1b). The pre-edge feature was then deconvoluted into pseudo-Voigt[36] (Figures 1c and 7b). The pseudo-Voigt function is often used to model the 1s−3d electronic transition[37] because of its Lorentzian and Gaussian contributions. The Lorentzian component of the pre-edge is due to the core−hole lifetime broadening of the selected edge, and the Gaussian component is related to the experimental broadening (e.g., source size, monochromator design, beamline optics, etc.). Therefore the pre-edge shape can be described by a Lorentzian function convoluted by a Gaussian function. The width of the Lorentzian contribution to the Voigt function has been chosen equal to 0.8 eV in accordance with the vanadium K-level width.[38] The widths of the Gaussian contribution have been considered as adjustable parameters and are comprised between 0.7 and 1.6 eV. The intensity ratio of the Lorentzian and Gaussian components was fixed to 1:1. It should be noted that width and height of the modeled pseudo-Voigt functions have little physical significance, being a convolution of two functions with significantly different width. Particular care was taken in using the smallest possible number of components in the pre-edge fitting procedure. No more than three peaks were fitted in the experimental spectra. The pre-edge information was derived by calculating the "total pre-edge peak area" (sum of the integrated area of each component), the "pre-edge peak centroid energy" (area-weighted average of the position in energy of each component), and the "pre-edge peak intensity" (maximum intensity of the net pre-edge peak) (Table 3).

Energy Resolution. XANES spectra were collected at three different beamlines, BL 11.1 and CRG-FAME for standard compounds and ID-21 for micro-XANES measurements, using two types of monochromator crystals with different d spacing, Si-(111) on BL 11.1 and ID-21 and Si-(220) on CRG-FAME. These monochromator crystals have different energy resolution. High- resolution experiments are achieved by using high-index Bragg reflections. The use of Si-(220) provides higher-energy resolution (intrinsic resolution of crystals equals to 0.28 eV at the V K-edge) than the use of Si-(111) (0.75 eV at the V K-edge). Other factors that influence energy resolution include the core-hole width at the K-edge (0.8 eV for the V K-edge[16]), the distance of the experiment from the X-ray source, source size, and vertical divergence, other storage ring characteristics (such as beam instability), and the size of energy steps used during a XANES spectral scan.[17] The energy resolution is an important factor when collecting V K-edge XANES spectra and especially when considering the pre-edge peak intensity. Pre-edge features could be very narrow, and if the experimental resolution is larger than their width, they may not be adequately resolved. We compared V K-edge spectra of standard compounds recorded using two different monochromator crystals. Differences in experimental conditions are responsible for differences in the pre-edge characteristics: pre-edge peak intensities obtained on beamline CRG-FAME (Si-(220)) are higher than those obtained on beamline BL 11.1. (Si-(111)) (Table 3). We then decided to normalize pre-edge peak characteristics (intensity and area) according value 1 for vanadinite compound (with the highest pre-edge peak) (Table 4). As shown in Table 4 by using this method (called "normalization step #2"), the standard deviation between the intensity and area values for the same sample recorded at different beamline has considerably decreased, giving evidence

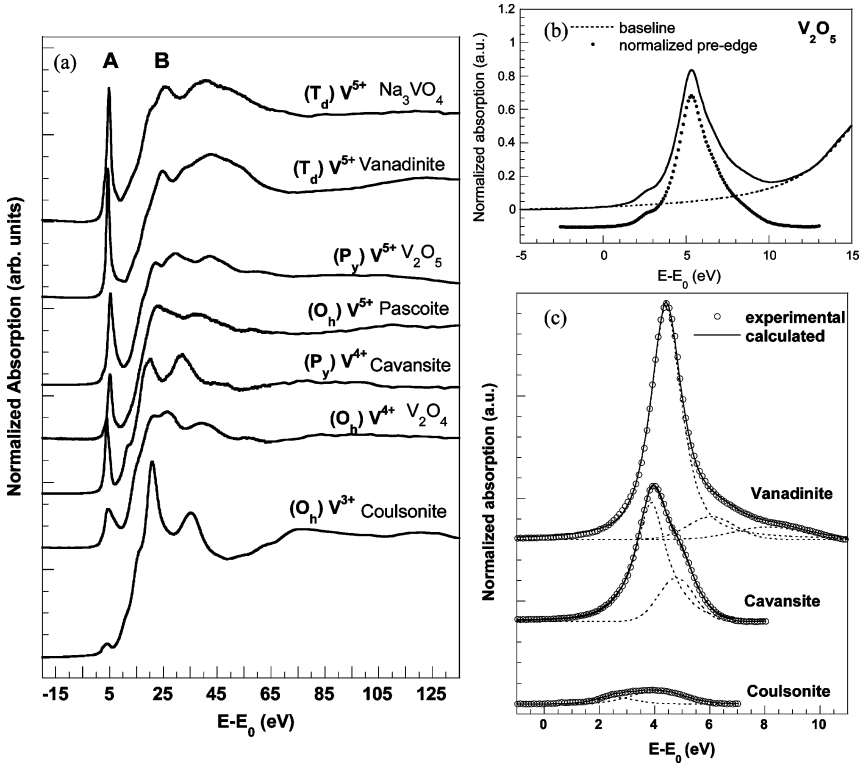

Figure 1. (a) Experimental V K-edge XANES spectra of standard compounds, in different oxidation state (i) and symmetry (s): (s)V^{i+} (recorded on beamline FAME, CRG-ESRF). (b) The pre-edge background was modeled with an interpolation function (baseline) using data a few electronvolts before and after the pre-edge. (c) Selected normalized pre-edge peak of standard compounds and the best model calculated with 1, 2, or 3 contributions.

TABLE 4: Normalized Pre-Edge Characteristics for V Standard Compounds According Value 1 for Vanadinite Characteristics (Method Called "Normalization Step #2")

	normalized intensity[a]		normalized area[a]	
sample	Si-(111)	Si-(220)	Si-(111)	Si-(220)
vanadinite	1	1	1	1
coulsonite	0.05	0.06	0.09	0.08
pascoite	0.52	0.48	0.51	0.52
V_2O_5	0.64	0.67	0.80	0.84
V_2O_4		0.27		0.56
cavansite		0.57		0.57
Na_3VO_4		0.99		1.06

[a] Data from Table 3 normalized according to value 1 for vanadinite information (intensity and total area).

to the reliability of our approach. Because pre-edge characteristics show only slight variations, V K-edge XANES spectra recorded on the three different beamlines can be compared.

Results and Discussion

Normalized XANES spectra for V standard compounds investigated in this study are shown in Figure 1a. A comparison among the spectra shows strong variations in energy position and intensity of the peaks both in the pre-edge region (before 15 eV) and in the edge region (after 15 eV).

Absorption Edge Position. Feature B (Figure 1a) is assigned to dipole-allowed 1s−4p transitions and is called absorption edge. The edge energy ($E_{1/2}$) of standard compounds (Figure 2 and Table 3) displays a positive shift with increase in the oxidation state of vanadium. The observed V K-edge energy shifts are consistent with those reported in the literature.[39−42] Such interpretation method is very easy to apply and does not require a long time. However the position of the absorption edge ($E_{1/2}$) overlaps in some case between several oxidation states (resulting in very large error bars in redox determination), and

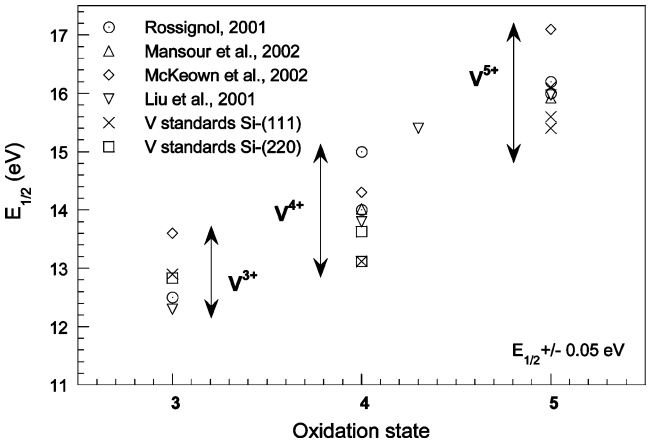

Figure 2. Edge energy $E_{1/2}$ (measured half way up the normalized edge step) vs oxidation state for standard compounds recorded at Elettra with a Si-(111) double crystal monochromator (×) and at ESRF on beamline CRG-FAME with a Si-(220) double crystal monochromator (□). Also are shown data from Rossignol et al.[42] 2001 ($V^{3+}{}_2O_3$, V^{4+}-OSO_4, $V^{4+}O_2$, $NH_4V^{5+}O_3$, $V^{5+}{}_2O_5$), Mansour et al.[40] 2002 ($V^{4+}O_2$, $V^{5+}{}_2O_5$), Liu et al.[39] 2001 ($V^{3+}{}_2O_3$, $V^{4+}O_2$,$V^{4.3+}{}_6O_{13}$, $V^{5+}{}_2O_5$), and McKeown et al.[41] 2002 (roscoelite V^{3+}, cavansite V^{4+}, vanadinite V^{5+}).

it becomes difficult to estimate rigorously the vanadium oxidation state. For example, if the edge energy position of an unknown sample is 13.5 eV, Figure 2 does not distinguish between V^{3+} and V^{4+}. The positive shift of the edge with the valence is related to the increased attraction of the 1s electron to the nucleus and reduced repulsive interactions (Coulomb interactions) with all the other electrons in the compounds. This valence effect shifts the whole spectrum. The problem is then to distinguish this shift from shifts due to other effects.[35,36] Features at the absorption edge are primarily sensitive to the valence and the local atomic surrounding the absorbing element (ligand type), but they are also affected by constructive and

destructive interferences (single and multiple scattering) arising from more distant neighbors around the central vanadium atoms, by a number of electronic many-body effects (e.g., quadrupolar transitions), and by changes in the medium- and long-range environment.[35]

This method based on interpolation schemes provides robust results only when it involves standard compounds with similar chemical bonding. For example, Wong et al.[10] obtained a well-correlated linear relation between the edge position (defined by the first peak in the derivative spectrum) and the valence regarding only vanadium oxides. They obtained a least-squares-fitted line with slope of 2.5 eV per valence. Rossignol et al.[20] estimated the error on the valence of ±0.4. Their results are based on a correlation obtained from various standards. Haskel et al.[43] established two separate correlations, from vanadium oxides and from molecular standards, with an error on the valence of ±0.25. When the local environment of vanadium is unknown, the edge position should be used as an indicator rather than an accurate method to determine the oxidation state. Although this interpretation method is easy to apply, it must be used with care.

Pre-Edge Features. The absorption edge itself is sometimes anticipated by pre-edge features. Pre-edge peaks are observed at approximately 5 eV (feature A, Figure 1a). In the present work, the pre-edge features have been analyzed following the procedure described previously to extract as much quantitative information as possible from the pre-edge features (Table 3). This pre-edge feature appears much less affected by changes in the medium- and long-range environment than the main edge region.

Pre-Edge Peak Intensity. The pre-edge peak intensity is a clear fingerprint of the symmetry change and is used to evaluate qualitatively the alteration of the vanadium local symmetry. A very intense pre-edge peak is observed for the vanadinite with tetrahedral V^{5+}, and the pre-edge peak becomes very weak in the case of regular octahedral symmetry as for coulsonite (Figure 1, Table 3). But this parameter is not sufficient to evaluate vanadium oxidation state as it is the case for chromium for which pre-edge peak is very weak for octahedral Cr^{3+} and very intense for tetravalent Cr^{6+}.[44] For vanadium compounds, each oxidation state (V^{3+}, V^{4+}, and V^{5+}) is associated to several symmetries (O_h, P_y, and T_d). The pre-edge peak intensities of standard compounds with the same oxidation state present large variations (Figure 3), as shown for V^{5+} standard compounds with various symmetry: O_h, P_y, or T_d. However, Sutton et al.[14] yielded that the plot of pre-edge peak intensity vs oxidation state shows a well-defined trend (third-order polynomial) in the case of glasses. They pointed out that the pre-edge peak intensity may be susceptible to changes due to symmetry variations, but they partially circumvented this complication by using standards of similar composition as the samples. As for the edge energy position, the intensity of the pre-edge peak provides robust results on the oxidation state only when it involves standard compounds with similar chemical bonding. We can note that Wong et al.[10] interpreted further the pre-edge features and established that the sharpness (half width × height) of the pre-edge peak has been correlated with the spread of V−O distances. They showed that this parameter depends on the size and distortion of the molecular cage around the vanadium absorber.

Pre-Edge Peak Centroid Position and Total Area. Examination of pre-edge features of standard compounds with vanadium at different valence symmetry reveals that different trends of pre-edge position vs pre-edge intensity can be observed (Figure 1). It suggests that both pre-edge peak energy and intensity might be exploited.

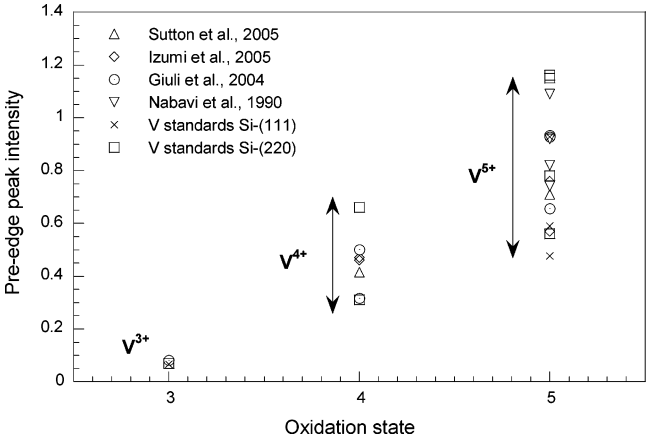

Figure 3. Pre-edge peak intensity (maximum intensity of the net pre-edge peak) vs oxidation state for standard compounds recorded at Elettra with a Si-(111) double crystal monochromator (×) and at ESRF on beamline CRG-FAME with a Si-(220) double crystal monochromator (□). Also shown are data from Sutton et al.[14] (V_2O_4, V_2O_5), Izumi et al.[48] ($Cr(T_d)V^{5+}O_4$, V_2O_5, $(P_y)V^{4+}OSO_4{\cdot}3H_2O$, V_2O_4), Giuli et al.[7] (vanadinite, descloizite $V^{5+}O_4$, V_2O_5, cavansite, V_2O_4 and $(O_h)V^{3+}$-magnetite), and Nabavi et al.[53] (V_2O_5, vanadinite, $CrVO_4$, $NH_4(T_d)$-$V^{5+}O_3$) (measurements performed with a Si-(111) double crystal monochromator).

Wong et al.[10] showed that a decrease of the vanadium oxidation state in oxides causes a negative shift of the pre-edge peak position. However generally, as for the intensity, the only pre-edge peak position does not provide reliable information on the oxidation state. Sutton et al.[14] yielded that the energy position of the pre-edge peak little evolves with the valence of vanadium in various glasses and especially between valence 4 and 5.

The normalized pre-edge peaks and their deconvolutions into 1:1 pseudo-Voigt components are shown in Figure 1c for selected standard compounds. The total area (sum of each component area) and the centroid position (area-weighted average of the position in energy of each component) are reported in Table 3. Characteristics of each component (deconvoluted data) are also reported in Table 3 (position and area). When vanadium is trivalent (coulsonite), the pre-edge peak can be fitted satisfactorily with two components, centered near 2.3−2.6 and 4 eV, respectively (Table 3), and the average centroid of the pre-edge peak is near 3.7 eV. For V^{4+} standard compounds, two components are also required to model pre-edge peaks, centered near 4 and 4.8−5.5 eV. But the centroid position depends on the vanadium symmetry. The centroid positions of V^{4+} with O_h and P_y symmetry are separated by ∼1 eV. For V^{5+} standard compounds, all spectra must be fitted with three components. V^{5+} standard compounds with different symmetry (O_h, P_y, and T_d) show variations on the position of each component, on its area and intensity. The total pre-edge area and intensity decrease from the most noncentrosymmetric geometry (T_d) to the octahedral geometry (Table 3). Sutton et al.[14] proposed an interpretation of the pre-edge peak structure for glasses by using the Z+1 model and by considering spin couple effects.[45] Their predictions indicate that, for glasses, three peaks are predicted for both V^{3+} and V^{4+} and two peaks are predicted for V^{5+}. These predictions are not consistent with the observed XANES for the chosen standard compounds, which are well crystallized. Two peaks are sufficient to fit pre-edge peaks of V^{3+} and V^{4+}, and a third peak has to be added to fit satisfactorily the pre-edge peak of V^{5+} standard compounds.

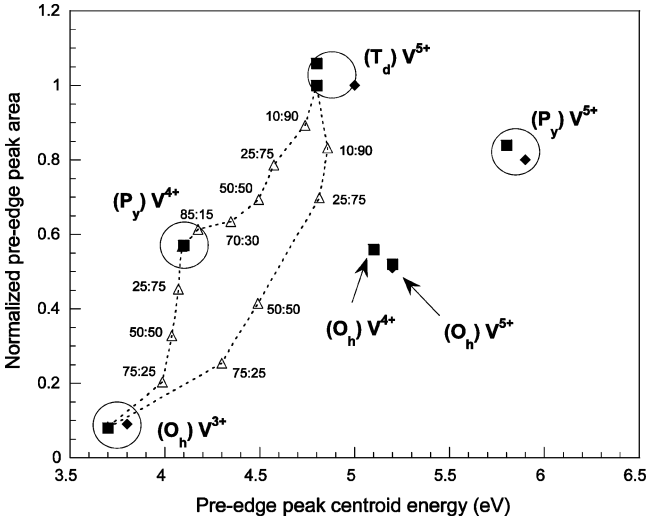

Figure 4. Total pre-edge peak area (normalized according value 1 to vanadinite) vs pre-edge peak centroid position. Black symbols refer to the standard compounds (■) recorded on beamline CRG-FAME and (♦) recorded at Elettra. The errors of the pre-edge centroid position are of the order of ±0.05 eV. Open triangles refer to modeled mixtures of $(O_h)V^{3+} + (P_y)V^{4+}$, $(P_y)V^{4+} + (T_d)V^{5+}$, and $(O_h)V^{3+} + (T_d)V^{5+}$, calculated for different mol % step.

Examination of the pre-edge parameters for all standard compounds (Table 3) suggests that the best approach to evaluate both vanadium oxidation state and symmetry consists of considering the pre-edge peak area (or intensity) as well as its centroid energy position. Noticeable changes occur in both energy position and total area (or intensity) of the pre-edge peak as a function of vanadium oxidation state and symmetry. Figure 4 shows that the data from the standard compounds lays in very distinct fields and it allows a rigorous discrimination of the oxidation state and symmetry of vanadium in an unknown sample. The pre-edge peak centroid position is exploited because it is more relevant than its absolute position (Table 3). The centroid position depends on the shape of the pre-edge peak and allows a better discrimination of the oxidation state and symmetry than the absolute pre-edge position. Nevertheless it is noteworthy that V^{4+} and V^{5+} compounds in an octahedral environment (V_2O_4 and pascoite respectively) are not well distinguished in Figure 4. But the compound V_2O_4 shows a wide pre-edge peak, and the stability of this compound could be discussed. The shape of this pre-edge peak could suggest a partial oxidation of initial V^{4+} to V^{5+} (indeed V^{5+} is the most stable form in an oxidized environment), which could explain that these compounds are not well separated. These results should be considered with caution.

Pre-edge peak areas are normalized according value 1 for vanadinite area. Pre-edge peak characteristics (area and centroid position) from spectra measured on different beamline present then only slight variations (Figure 4), slighter than changes which occur with oxidation state and symmetry variations.

Effects of the Mixture of Vanadium Oxidation State (Multivalency) and Symmetry on the Pre-Edge Features. To examine the effect of mixed vanadium oxidation state and/or symmetry, we collected V K-edge XANES spectrum for a mixture of standard compounds (cavansite and vanadinite) containing square pyramidal $(P_y)V^{4+}$ and tetrahedral $(T_d)V^{5+}$. The mixture was prepared on a molar basis with respect to only V atoms (70:30 mixture (in mol % V) of $(P_y)V^{4+}$ and $(T_d)V^{5+}$). This was done to simulate the variation of the pre-edge with variation of oxidation state and/or structural site. We compared the measured pre-edge spectrum of this experimental mixture with those derived from calculated linear combinations of the normalized XANES spectra of the respective end members. The calculated pre-edge spectrum for the mixture 70:30 of cavansite/vanadinite compares well with that measured experimentally (Figure 5), suggesting that the calculated pre-edges are representative of the experimental ones. The centroid energy and the area of the calculated pre-edge peaks are reported in Figure 4 as open triangles. It can be clearly seen that the trends reported in Figure 4 are markedly nonlinear, as previously noted by Wilke et al.[20] and O'Day et al.[46] for the Fe K-edge. These authors explained that the most nonlinear variations in both centroid and intensity were observed when both the oxidation state and the symmetry of iron vary simultaneously.

Such a simulation might not be absolutely exact because of nonlinear effects. XANES fits using linear combinations do not account sufficiently for nonlinear absorption in mixtures when the end-members components have very different mass absorptions (different densities and absorption characteristics). O'Day et al.[46] have precisely studied iron speciation in natural mixtures, and they have shown that the relative proportions of each component of the total spectrum depend on the local bonding environment(s) around the element of interest, on the type and number of components in the mixture, and on the composition of the matrix. They noted that the observed differences between

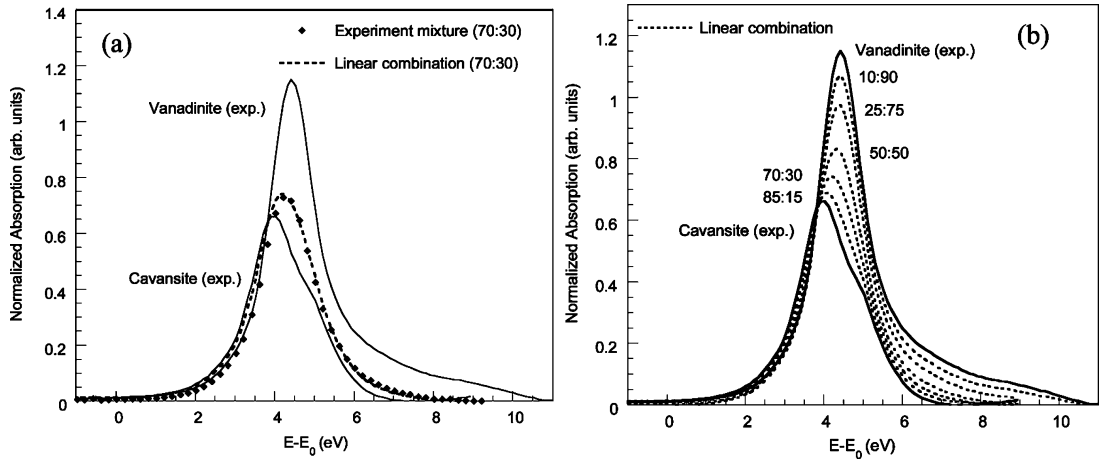

Figure 5. (a) Normalized pre-edge peak of the 70:30 experimental mixture of cavansite plus vanadinite compared to the normalized pre-edge peak derived from calculated linear combination (70:30) of the normalized XANES spectra of the respective end members (all mixtures are in terms of mol % V). (b) Normalized pre-edge peaks derived from various calculated linear combinations of the normalized XANES spectra of cavansite and vanadinite.

TABLE 5: Pre-Edge Information of the Steel Slag (Micro-XANES on Beamline ID21 at ESRF)

	pre-edge peak[a]				main edge	
sample	centroid (eV)	absolute position (eV)	normalized intensity	total area	$E_{1/2}$ (eV)	oxidation state and symmetry[b]
ROI 1	4.8	4.8	1.03	2.17	16.5	5^+ T_d
ROI 2	4.7	4.7	0.94	1.92	15.9	most of 5^+ T_d
ROI 3	4.5	4.8	0.44	0.96	14.9	3^+ O_h + 5^+ T_d
ROI 4	4.1	4.4	0.33	0.52	13.3	most of 3^+ O_h
ROI 5	4.3	4.5	0.26	0.56	13.4	most of 3^+ O_h
ROI 6	4.0	4.6	0.11	0.30	13.2	3^+ O_h
ROI 7	4.3	4.5	0.49	1.10	15.0	3^+ O_h + 5^+ T_d
ROI 8	4.6	4.5	0.57	1.16	15.8	3^+ O_h + 5^+ T_d
ROI 9	4.7	4.8	1.24	2.24	16.7	5^+ T_d

[a] Normalized and fitted according to the procedure described previously ("normalization step #2" not applied). [b] From XANES determination (see Figure 8), octahedral (O_h) and tetrahedral (T_d) symmetry. The errors of the energy is of the order of ±0.05 eV.

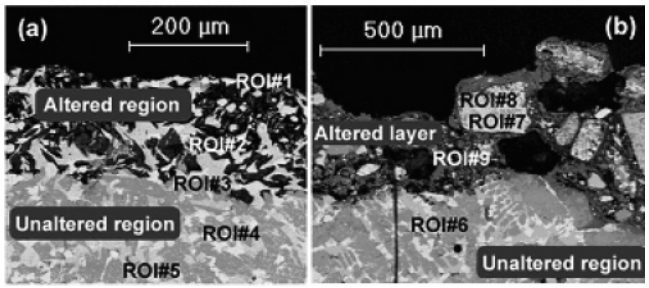

Figure 6. SEM-BSE micrographs of polished steel slag grains embedded in epoxy resin and previously leached at a laboratory scale (a) and in lysimeter (b). ROI selected to record micro-XANES spectra with the focused X-ray beam are indicated (ROI 1−9). ROI 4−6 are in the unaltered region, ROI 1, 2, and 9 are in the altered region, and ROI 3, 7, and 8 are in little altered regions.

true and apparent fractions depend on the total fluorescence yield of the iron in the compound, which is proportional to the mass fraction of iron in the compounds, and on matrix absorption and fluorescence. So fluorescence intensities of complex mixtures can be influenced significantly by sample and matrix absorption that does not vary in a simple linear fashion as a function of concentration. This study suggests that calibration curves should be constructed on a case-by-case basis if component fractions of complex mixtures have to be determined quantitatively from XANES fits and it points out the importance of a high-quality, experimentally consistent with standard compounds library. In our study, the good agreement between true and apparent fractions may be due to a low matrix effects. Indeed, the linear combinations were calculated with spectra of standard compounds diluted in BN for transmission mode. The BN dilution certainly mitigates the matrix effects.

A Case Study: Vanadium Oxidation State and Symmetry within Altered Steel Slag. Analysis of the pre-edge features of standard compounds showed that it is possible to derive information on the vanadium speciation (oxidation state and symmetry) from the centroid position and the total area of the pre-edge peak. When studying vanadium speciation in unknown sample as steel slag, variations in the symmetry and in the oxidation state can be expected due to the different altered areas. This makes the analysis of the pre-edge much more challenging. A very high signal-to-noise ratio, the best experimental resolution possible, and a careful pre-edge peak examination with the appropriate interpretative methods are required.

The oxidation state and symmetry of vanadium in leached steel slag were determined using the method presented previ-

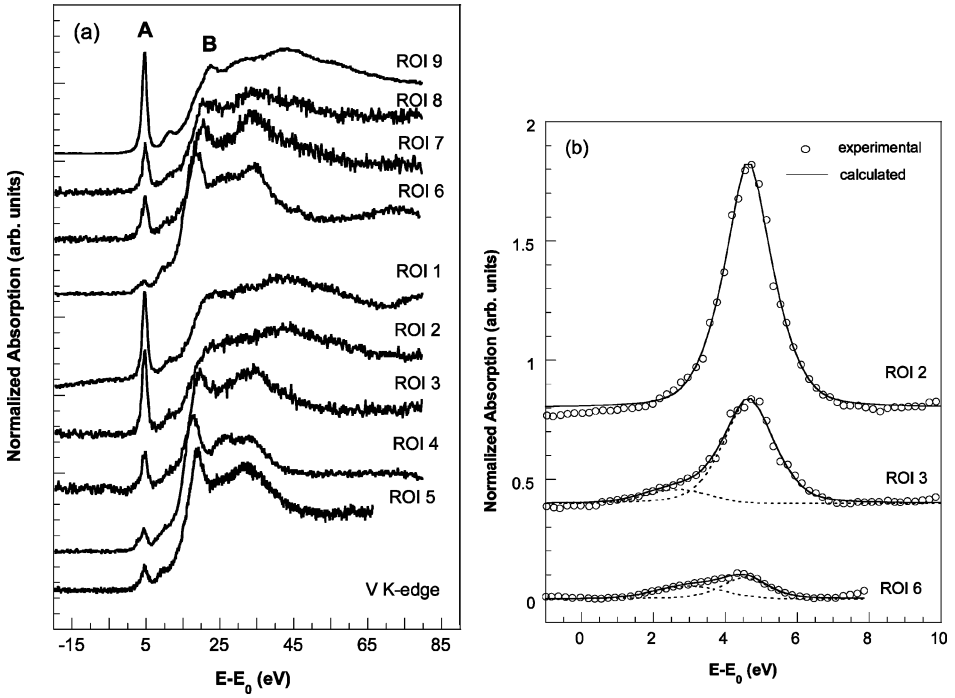

Figure 7. (a) Experimental V K-edge micro-XANES spectra of steel slag (ROI 1−9). (b) Selected normalized pre-edge peak and the best model calculated with 1 or 2 contributions.

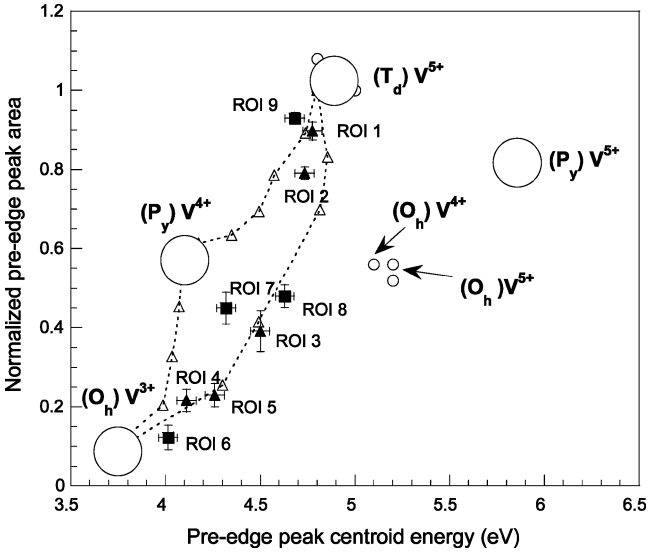

Figure 8. Total pre-edge peak area vs. pre-edge peak centroid position. White circles refer to standard compounds and black symbols to micro-XANES measurements in leached steel slag (in CTG Leachcrete (▲) or in lysimeter (■)).The errors of the pre-edge centroïd position are of the order of ±0.05 eV. The major error source on the pre-edge peak area comes from the background modeling (baseline) and the normalization procedure. Open triangles refer to modeled mixture with several vanadium oxidation states (multivalency) and symmetries, calculated for different mol% step (see Figure 4).

ously based on pre-edge analysis (Figure 4) and correlations between centroid position and normalized area. The altered steel slag is a heterogeneous matrix at the micrometer scale, in term of vanadium valence and symmetry distribution. Bulk-XANES measurements are then inadequate to assess accurately the variation of the oxidation state and symmetry. We have recorded micro-XANES spectra to elucidate the microdistribution of vanadium in steel slag from the unaltered to the altered layer. Several ROI were selected to record micro-XANES spectra with the focused beam (Figures 6 and 7). Because of a high vanadium release during laboratory-scale leaching tests,[27] the oxidation of vanadium was suspected. Moreover since V^{5+} exhibits some toxicity,[47] it is crucial to evaluate the oxidation state of vanadium within altered steel slag in terms of environmental impacts especially if steel slag is reused as an aggregate in road constructions. The results (Figure 8) show that vanadium is mainly present in unaltered region as octahedral V^{3+} (ROI 4−6). A significant increase of the pre-edge peak area is observed as well as a slight positive shift of its centroid position for ROI 1, 2, and 9. It reflects the loss of symmetry of the vanadium site and its oxidation during leaching. Vanadium is present in altered region in the pentavalent form with tetrahedral symmetry. Then Figure 8 shows that vanadium is present in little altered region (ROI 3, 7, and 8) as a mixture of various oxidation state and symmetry but does not allow a rigorous discrimination of the nature of the mixture. However, the correspondence with the mixing curve coulsonite/vanadinite suggests that vanadium is present as a mixture of octahedral V^{3+} and tetrahedral V^{5+} (around 50:50 mixture), showing the complexity of vanadium oxidation state distribution in leached steel slag. But the calibration curve (open triangles in Figure 4) is then not well-adapted because of matrix variation between XANES spectra of standard compounds and micro-XANES spectra collected in fluorescence mode.[46] So this observation cannot be quantitatively confirmed.

Micro-XANES results (Figure 8) shows the distribution of vanadium forms at the sub-micrometer level in altered steel slag and their evolution during leaching. These results suggest that the vanadium speciation is different in altered or unaltered region. They provide essential information to explain vanadium release and to identify the mechanisms associated. We have chosen various standard compounds in the type of coordinating atom (oxides, minerals). The choice of standard compounds should be always done with care, and standard compounds with similar chemical bonding are preferred. However, the nature of standard compounds appears less crucial with this selected interpretation method. This method is well adapted to the assessment of vanadium speciation in a heterogeneous unknown sample, such as steel slag, even with standard compounds with different chemical bonding.

Conclusion

The pre-edge peak is the most useful feature in the XANES spectra to determine both the oxidation state and symmetry of vanadium present in an unknown heterogeneous sample, such as leached steel slag. We have seen that it is possible to derive information on vanadium speciation from the pre-edge peak centroid position if the influence of the vanadium symmetry (through the pre-edge peak area) is taken into account. The pre-edge analysis procedure presented is laborious but provides more accurate and reliable data than others interpretation methods based on the absorption edge energy position and/or on the pre-edge peak intensity. The selected procedure was previously developed by Wilke et al. for Fe K-edge,[20] and we demonstrated in this paper that it is also well adapted for V K-edge.

Acknowledgment. This work was supported by the French Agency for Environment and Energy Management and the French Institute of Industrial Environment and Risks. LCPC is acknowledged for providing BOF steel slag samples.

References and Notes

(1) Peacock, C. L.; Sherman, D. M. *Geochim. Cosmochim. Acta* **2004**, *68*, 1723.
(2) Wanty, R. B.; Goldhaber, M. B. *Geochim. Cosmochim. Acta* **1992**, *56*, 1471.
(3) Schindler, M.; Hawthorne, F. C.; Baur, W. H. *Chem. Mater.* **2000**, *12*, 1248.
(4) Evans, H. T. Vanadium. In *Handbook of Geochemistry*; Springer-Verlag, Ed.; Springer-Verlag: Berlin, 1969; Vol.II/1, sec. 23, part A.
(5) Schindler, M.; Hawthorne, F. C. *The Canadian Mineralogist* **2000**, *38*, 1443.
(6) Zavalij, P. Y.; Whittingham, M. S. *Acta Crystallogr.* **1999**, *B55*, 627.
(7) Giuli, G.; Paris, E.; Mungall, J.; Romano, C.; Dingwell, D. *Am. Mineral.* **2004**, *89*, 1640.
(8) Brown, G. E. J.; Calas, G.; Waychunas, G. A.; Petiau, J. X-ray absorption spectroscopy: applications in mineralogy and geochemistry. In *Reviews in Mineralogy. Spectroscopic Methods in Mineralogy and Geology*; Hawthorne, F. C., Ed.; Mineralogical Society of America: Chelsea, 1988; Vol. 18; pp 431.
(9) Bianconi, A. *EXAFS and Near Edge Structure*; A. Bianconi, L. I. S. S., Ed.; Springer: Berlin, 1983; p 118.
(10) Wong, J.; Lytle, F. W.; Messmer, R. P.; Maylotte, D. H. *Phys. Rev. B* **1984**, *30*, 5596.
(11) Rehr, J. J.; Albers, R. C. *Rev. Mod. Phys.* **2000**, *72*, 621.
(12) Roe, A. L.; Schneider, D. J.; Mayer, R. J.; Pyrz, J. W.; Widom, J.; Que, L. *J. Am. Chem. Soc.* **1984**, *106*, 1676.
(13) Glatzel, P.; Yano, J.; Bergmann, U.; Visser, H.; Robblee, J. H.; Gu, W.; de Groot, F. M. F.; Cramer, S. P.; Yachandra, V. K. *J. Phys. Chem. Solids* **2005**, *66*, 2163.
(14) Sutton, S. R.; Karner, J.; Papike, J.; Delaney, J. S.; Shearer, C.; Newville, M.; Eng, P.; Rivers, M.; Dyar, M. D. *Geochim. Cosmochim. Acta* **2005**, *69*, 2333.
(15) Peterson, M. L.; Brown, G. E. J.; Parks, G. A. *Proc. Mater. Res. Soc. Spring Mtg. San Francisco* **1996**, 75.
(16) Farges, F. *J. Non-Cryst. Solids* **1996**, *204*, 53.
(17) Farges, F.; Brown, G. E. J.; Rehr, J. J. *Geochim. Cosmochim. Acta* **1996**, *60*, 3023.

(18) Farges, F.; Lefrère, Y.; Rossano, S.; Berthereau, A.; Calas, G.; Brown, G. E. J. *J. Non-Cryst. Solids* **2004**, *344*, 176.
(19) Passerini, S.; H. Smyrl, W.; Berrettoni, M.; Tossici, R.; Rosolen, M.; Marassi, R.; Decker, F. *Solid State Ionics* **1996**, *90*, 5.
(20) Wilke, M.; Farges, F.; Petit, P. E.; Brown, G. E. J.; Martin, F. *Am. Mineral.* **2001**, *86*, 714.
(21) Wilke, M.; Partzsch, G. M.; Bernhardt, R.; Lattard, D. *Chem. Geol.* **2004**, *213*, 71.
(22) Petit, P.-E.; Farges, F.; Wilke, M.; Solé, V. A. *J. Synchrotron Radiat.* **2001**, *8*, 952.
(23) Geiseler, J. *Waste Manage.* **1996**, *16*, 59.
(24) Presslinger, H.; Antlinger, K.; Klepp, K. O.; Hiebler, H. *Steel Res.* **1997**, *68* (12), 520.
(25) Maxl, E.; Hiebler, H.; Presslinger, H.; Antlinger, K. *ISIJ Int.* **1993**, *33* (1), 88.
(26) Proctor, D. M.; Fehling, K. A.; Shay, E. C.; Wittenborn, J. L.; Avent, C.; Bigham, R. D.; Connolly, M.; Lee, B.; Shepker, T. O.; Zak, M. A. *Environ. Sci. Technol.* **2000**, *34*, 1576.
(27) Chaurand, P.; Rose, J.; Briois, V.; Olivi, L.; Hazemann, J. L.; Proux, O.; Domas, J.; Bottero, J. Y. *J. Hazard. Mater.* **2007**, *B139*, 537−542.
(28) Wehrli, B.; Stumm, W. *Geochim. Cosmochim. Acta* **1988**, *53*, 69.
(29) Moudilou, E.; Bellotto, M.; Defosse, C.; Serclerat, I.; Baillif, P.; Touray, J. C. *Waste Manage.* **2002**, *22*, 153.
(30) Proux, O.; Biquard, X.; Lahera, E.; Menthonnex, J. J.; Prat, A.; Ulrich, O.; Soldo, Y.; Trévisson, P.; Kapoujyan, G.; Perroux, G.; Taunier, P.; Grand, D.; Jeantet, P.; Deleglise, M.; Roux, J. P.; Hazemann, J. L. *Phys. Scr.* **2005**, *115*, 970.
(31) Proux, O.; Nassif, V.; Prat, A.; Ulrich, O.; Lahera, E.; Biquard, X.; Menthonnex, J. J.; Hazemann, J. L. *J. Synchrotron Radiat.* **2006**, *13*, 59.
(32) Susini, J.; Salome, M.; Fayard, B.; Ortega, R.; Kaulich, B. *Surf. Rev. Lett.* **2002**, *9*, 203.
(33) Bearden, J. A.; Burr, A. F. *Rev. Mod. Phys.* **1967**, *39*, 125.
(34) Galoisy, L.; Calas, G.; Arrio, M. A. *Chem. Geol.* **2001**, *174*, 307.
(35) Farges, F. *Phys. Rev. B* **2005**, *71*, 155109 1.
(36) Poumellec, B.; Marucco, J. F.; Touzelin, B. *Phys. Rev. B* **1987**, *35*, 2284.
(37) Mysen, B. O.; Virgo, D.; Scarfe, C. M.; Cronin, D. J. *Am. Mineral.* **1985**, *70*, 487.
(38) Keski Rahkonen, O.; Krause, M. O. *At. Data Nucl. Data Tables 14* **1974**, *139*.
(39) Liu, R. S.; Cheng, Y. C.; Gundakaram, R.; Jang, L. Y. *Mater. Res. Bull.* **2001**, *36*, 1471.
(40) Mansour, A. N.; Smith, P. H.; Baker, W. M.; Balasubramanian, M.; McBreen, J. *Electrochim. Acta* **2002**, *47*, 3151.
(41) McKeown, D. A.; Muller, I. S.; Matlack, K. S.; Pegg, I. L. *J. Non-Cryst. Solids* **2002**, *298*, 160.
(42) Rossignol, C.; Ouvrard, G. *J. Power Sources* **2001**, *97*−*98*, 491.
(43) Haskel, D.; Islam, Z.; Lang, J.; Kmety, C.; Srajer, G. *Phys. Rev. B* **2004**, *70*, 054422.
(44) Peterson, M. L.; Brown, G. E. J.; Parks, G. A.; Stein, C. L. *Geochim. Cosmochim. Acta* **1997**, *61*, 3399.
(45) Westre, T. E.; Kennepohl, P.; DeWitt, J. G.; Hedman, B.; Hodgson, K. O.; Solomon, E. I. *J. Am. Chem. Soc.* **1997**, *119*, 6297.
(46) O'Day, P. A.; Rivera, Jr., N.; Root, R.; Carroll, S. A. *Am. Mineral.* **2004**, *89*, 572.
(47) Mukherjee, B.; Patra, B.; Mahapatra, S.; Banerjee, P.; Tiwari, A.; Chatterjee, M. *Toxicol. Lett.* **2004**, *150*, 135.
(48) Izumi, Y.; Kiyotaki, F.; Yagi, N.; Vlaicu, A.-M.; Nisawa, A.; Fukushima, S.; Yoshitake, I.; Iwasawa, Y. *J. Phys. Chem. B* **2005**, *109*, 14884.
(49) Takemoto, K.; Ueki, T.; Fayard, B.; Yamamoto, A.; Salomé, M.; Scippa, S.; Susini, J.; Uyama, T.; Michibata, H.; Kihara, H. *J. Phys. IV* **2003**, *104*.
(50) Asbrink, S. *J. Appl. Crystallogr.* **1986**, *19*, 331.
(51) Kusthardt, U.; Hedman, B.; Hodgson, K. O.; Hahn, R.; Yilter, H. *FEBS Lett.* **1993**, *329*, 5.
(52) Denis, S.; Baudrin, E.; Orsini, F.; Ouvrard, G.; Touboul, M.; Tarascon, J.-M. *J. Power Sources* **1999**, *81*−*82*, 79.
(53) Nabavi, M.; Taulelle, F.; Sanchez, C.; Verdaguer, M. *J. Phys. Chem. Solids* **1990**, *51*, 1375.
(54) Zhang, Q.; Yang, W.; Wang, X.; Wang, Y.; Shishido, T.; Takehira, K. *Microporous Mesoporous Mater.* **2005**, *77*, 223.
(55) Yang, Y.; Lim, S.; Wang, C.; Harding, D.; Haller, G. *Microporous Mesoporous Mater.* **2004**, *67*, 245.
(56) Laruelle, S.; Poizot, P.; Baudrin, E.; Briois, V.; Touboul, M.; Tarascon, J.-M. *J. Power Sources* **2001**, *97*−*98*, 251.
(57) Rose, J.; Benard, A.; Susini, J.; Borschneck, D.; Hazemann, J. L.; Cheylan, P.; Vichot, A.; Bottero, J. Y. *Environ. Sci. Technol.* **2003**, *37*, 4864.
(58) Jackson, W. E.; Farges, F.; Yeager, M.; Mabrouk, P. A.; Rossano, S.; Waychunas, G. A.; Solomon, E. I.; Brown, G. E. J. *Geochim. Cosmochim. Acta* **2005**, *69*, 4315.
(59) Chichagov, A. V. *Kristallographiya* **1990**, *35* (3), 610.
(60) Evans, H. T. *Am. Mineral.* **1973**, *58*, 412.
(61) Hughes, J. M.; Schindler, M.; Francis, C. A. To be submitted, 2005.
(62) Hardcastle, F. D.; Wachs, I. E. *J. Phys. Chem.* **1991**, *95*, 5031.
(63) Dai, Y.; Hugnes, J. *Can. Mineral.* **1989**, *27*, 189.